Increases in blood glucose levels also have pathological effects that seem to be strongly correlated to SN and have potentially important implications for diabetes. The locomotor activity of experimental animals is closely related to the activity of dopamine-containing neurons (*20*). Yet, the ambulatory activity of streptozotocin-induced diabetic rats is decreased when the blood glucose level rises (*21*). We would like to propose that high glucose levels inhibit $K_{ATP}$ channels, depolarize SN terminals, increase GABA release, and thereby also extensively inhibit the activity of dopaminergic neurons (*21*), resulting in a decrease of ambulatory activity.


REFERENCES AND NOTES

1. P. R. Stanfield, *Trends Neurosci.* **10**, 335 (1987).
2. O. H. Petersen and I. Findlay, *Physiol. Rev.* **67**, 1054 (1987).
3. F. M. Ashcroft, *Annu. Rev. Neurosci.* **11**, 97 (1988).
4. J. R. De Weille, H. Schmid-Antomarchi, M. Fosset, M. Lazdunski, *Proc. Natl. Acad. Sci. U.S.A.* **85**, 1312 (1988).
5. M. J. Dunne *et al.*, *EMBO J.* **8**, 413 (1989).
6. J. R. De Weille, H. Schmid-Antomarchi, M. Fosset, M. Lazdunski, *Proc. Natl. Acad. Sci. U.S.A.* **86**, 2971 (1989).
7. H. Schmid-Antomarchi, J. R. De Weille, M. Fosset, M. Lazdunski, *J. Biol. Chem.* **262**, 15840 (1987).
8. N. C. Sturgess, M. L. J. Ashford, D. L. Cook, C. N. Hales, *Lancet* **ii**, 474 (1985).
9. H. Bernardi, M. Fosset, M. Lazdunski, *Proc. Natl. Acad. Sci. U.S.A.* **85**, 9816 (1988).
10. C. Mourre, Y. Ben Ari, H. Bernardi, M. Fosset, M. Lazdunski, *Brain Res.* **486**, 159 (1989).
11. J. H. Fallon and S. E. Loughlin, in *The Rat Nervous System*, G. Paxinos, Ed. (Academic Press, San Diego, 1985), vol. 1, pp. 353–374.
12. Wistar rats (200 g) were killed by decapitation, and their brains were rapidly removed. SN slices (0.7 mm) were dissected with a McIlwain chopper and rapidly incubated in medium previously gassed with 95% $O_2$ and 5% $CO_2$ and containing 120 m*M* NaCl, 3.5 m*M* KCl, 1 m*M* $MgSO_4$, 16 m*M* $NaHCO_3$, 1.2 m*M* $CaCl_2$, 10 m*M* D-glucose in 11 m*M* Hepes-NaOH buffer (*p*H 7.4) at 37°C. Slices were gassed for 90 min before the beginning of experiments in order to permit a full recovery. Aeration was continuous during the whole procedure. Slices were preloaded for 20 min with 1 μ*M* [$^3$H]GABA (2 μCi/ml) in 1 ml of medium in the presence of 50 μ*M* aminooxyacetic acid to inhibit GABA transaminase. A 45-min washing was done before beginning the release experiments. Then one slice was transferred per well of a multiwell box (1 ml of oxygenated medium per well). [D. Minc-Golomb, Y. Levy, N. Kleinberger, M. Schramm, *Brain Res.* **402**, 255 (1987)]. Release experiments were then carried out during consecutive intervals of 5 min for 40 to 50 min. Eight independent experiments were performed at the same time. Fractional rates of release were calculated as [$^3$H]GABA released during each 5-min interval and expressed as the percentage of the [$^3$H]GABA content in the tissue at the beginning of the respective intervals.
13. Slices were loaded for 30 min with 5 to 10 μCi/ml of $^{86}Rb^+$. A 30-min washing was carried out before the $^{86}Rb^+$ efflux was started. Experiments were then performed as for [$^3$H]GABA release. Effectors were added as described in the figures. For anoxic conditions we used 95% $N_2$/5% $CO_2$ instead of 95% $O_2$/5% $CO_2$; 10 m*M* glucose was used in each case. Intracellular ATP depletion was obtained when necessary by adding oligomycin (2.4 μg/ml) and 1 m*M* 2DG (*8*) in incubation medium without glucose and in $O_2$/$CO_2$ conditions. After solubilizing the slices with 1% Triton X-100, total $[ATP]_{in}$ was measured with the luciferase-luciferin technique [R. Christen, R. W. Schackman, B. M. Shapiro, *J. Biol. Chem.* **258**, 5392 (1983)]. Proteins were measured [M. M. Bradford, *Anal. Biochem.* **72**, 248 (1976)] with bovine serum albumin as standard.
14. C. F. Saller and L. A. Chiodo, *Science* **210**, 1269 (1980).
15. M.-L. Smith, H. Kalimo, D. S. Warner, B. K. Siesjö, *Acta Neuropathol.* **76**, 253 (1988).
16. K. Gale, *Fed. Proc.* **44**, 2414 (1985).
17. ———, *Adv. Neurol.* **44**, 343 (1986).
18. G. Nevander, M. Ingvar, R. N. Auer, B. K. Siesjö, *Ann. Neurol.* **18**, 281 (1985).
19. M. Saji and D. J. Reis, *Science* **235**, 66 (1987).
20. D. C. Hoffman and R. J. Beniger, *Pharmacol. Biochem. Behav.* **22**, 341 (1985).
21. Y. Shimomura *et al.*, *Endocrinology* **123**, 2621 (1988).


22. We thank Hoechst-Roussel Pharmaceuticals for gifts of glibenclamide, tolbutamide, LH32, and LH35; Boehringer Ingelheim for gliquidone; Pfizer for glipizide; and Schering-Plough for glisoxepide. We thank F. Aguila and C. Roulinat-Bettelheim for technical assistance. Supported by the Centre National de la Recherche Scientifique and the Institut National de la Santé et de la Recherche Médicale (CRE n° 88.2007). S.A. is supported by a French Foreign Ministry fellowship.

29 September 1989; accepted 22 December 1989


# Functional Properties of Rat Brain Sodium Channels Expressed in a Somatic Cell Line


TODD SCHEUER, VANESSA J. AULD, SHELLEY BOYD, JAMES OFFORD, ROBERT DUNN, WILLIAM A. CATTERALL



**Transfection of Chinese hamster ovary cells with complementary DNA encoding the $R_{IIA}$ sodium channel α subunit from rat brain led to expression of functional sodium channels with the rapid, voltage-dependent activation and inactivation characteristic of sodium channels in brain neurons. The sodium currents mediated by these transfected channels were inhibited by tetrodotoxin, persistently activated by veratridine, and prolonged by *Leiurus* α-scorpion toxin, indicating that neurotoxin receptor sites 1 through 3 were present in functional form. The $R_{IIA}$ sodium channel α subunit cDNA alone is sufficient for stable expression of functional sodium channels with the expected kinetic and pharmacological properties in mammalian somatic cells.**


SODIUM CHANNELS MEDIATE THE MAJOR inward current responsible for the upstroke of the action potential in many excitable cells. Rat brain $Na^+$ channels are heterotrimeric proteins consisting of α, $\beta_1$, and $\beta_2$ subunits of 260, 36, and 33 kD, respectively (*1*). A wide variety of neurotoxins affect $Na^+$ channel activity, and five different toxin receptor sites on the rat brain channel have been biochemically characterized (*1*). Three distinct subtypes of the rat brain $Na^+$ channel α subunit, $R_I$, $R_{II}$, and $R_{III}$, have been cloned and sequenced (*2, 3*). Expression of α subunits by injection of mRNA into *Xenopus* oocytes has shown that many $Na^+$ channel functions are mediated by the α subunit alone (*4–7*). However, high molecular weight brain mRNA or $R_{IIA}$ mRNA direct the synthesis of $Na^+$ channels with unusually slow inactivation kinetics (*7*). Coexpression with size-fractionated brain mRNA smaller than 4 kb is able to accelerate inactivation, suggesting that a low molecular weight brain protein is necessary for rapid inactivation in oocytes (*7*). We have stably expressed cDNA for the $R_{IIA}$ α subunit in Chinese hamster ovary (CHO) cells, a mammalian cell line that lacks endogenous voltage-sensitive $Na^+$ channels, in order to examine the physiological and pharmacological properties of these channels in the genetic background of a mammalian somatic cell.

CHO cells were cotransfected (*8*) with pVA222 containing the coding region of the $R_{IIA}$ $Na^+$ channel α subunit (*7*) in vector pECE (*9*) and pSV2neo, a plasmid conferring resistance to the antibiotic G418. Control transfections with pECE lacking the α subunit were also performed. Transfectants were selected through multiple passages in the presence of G418 (*8*). Seven independent stable G418-resistant cell lines were isolated and analyzed for the presence of the α subunit transcript by the ribonuclease (RNase) protection procedure. Cell lines PVA1 and PVA4 expressed RNA that protected a 781-nucleotide (nt) cRNA antisense transcript covering nucleotides 50 to 831 of the $R_{IIA}$ 5′ region (*7*) (Fig. 1A). Northern (RNA) blots showed that these two cell lines expressed mRNA species of approximately 7.5 and 3.5 kb, which were specifically recognized by an $R_{IIA}$ cRNA probe (Fig. 1B, lanes 3 and 4). Although 7.5 kb is the expected size for transcription of the $R_{IIA}$ cDNA in the pECE vector, the 3.5-kb species is truncated, possibly due to premature termination of transcription or


T. Scheuer, J. Offord, W. A. Catterall, Department of Pharmacology, School of Medicine, University of Washington, Seattle, WA 98195.
V. J. Auld, S. Boyd, R. Dunn, Department of Medical Genetics, University of Toronto, Toronto, Ontario, Canada M5S 1A1.

**Table 1.** Mean values for $Na^+$ currents in transfected cells. The number in parentheses is *n*.

| Cell line | Fraction of active cells ($I_{Na}$ > 20 pA) | Mean $I_{Na}$ (pA) | Activation* | | Inactivation* | |
|---|---|---|---|---|---|---|
| | | | $V_{0.5}$ (mV) | *k* | $V_{0.5}$ (mV) | *k* |
| CP1 | 0/6 | | | | | |
| PVA1 | 43/61 | 148 ± 8 (19) | −0.7 ± 0.9 (8) | −9.1 ± 0.5 (8) | −46.5 ± 0.5 (9) | 4.6 ± 0.4 (9) |
| PVA4 | 19/22 | 150 ± 5 (8) | | | | |

*Activation and inactivation curves were derived as described in the legend to Fig. 2B.

abnormal RNA splicing within the cDNA expression unit. Cell line CP1, which was transfected with vector only, did not have detectable levels of mRNA encoding $Na^+$ channels (Fig. 1B, lane 2). In contrast to the transfected cells, rat brain neurons express the full-length α subunit mRNA of 9.0 kb (Fig. 1B, lane 1). Variation of the input RNA to give comparable hybridization signals indicated that α subunit mRNA was approximately 10% as abundant in transfected cells as in rat brain. The RNase protection experiments, which are sensitive to even single nucleotide differences, confirm that the mRNA expressed in these cells is transcribed from transfected $R_{IIA}$ cDNA.

The expression of functional channels on the cell surface was assayed by whole cell voltage clamp (*10, 11*). Cells of the two α subunit–transfected cell lines, PVA1 and PVA4, generated inward currents that activated and then inactivated within 2 ms in response to depolarizing voltage steps of increasing size (Fig. 1C). Control transfectants (CP1 cells) did not produce a similar voltage-activated inward current (Fig. 1C and Table 1). Voltage-activated inward currents were observed in greater than 70% of the PVA1 and PVA4 cells (Table 1). The properties of these inward currents remained stable through more than 27 passages.

The voltage-activated inward currents in transfected cells were reversibly blocked by 80% in the presence of 100 n*M* tetrodotoxin (TTX) (Fig. 1D) and completely blocked by 200 n*M* TTX ($n$ = 3). The presence of these currents only in transfected cells, their inhibition by TTX, their rapidly inactivating time course, and their reversal potential near +70 mV indicated that they were mediated by $Na^+$ channels encoded by the transfected $R_{IIA}$ cDNA clone.

The mean peak $Na^+$ current was approximately 150 pA in both PVA1 and PVA4 cells (Table 1), corresponding to the simultaneous activation of approximately 140 $Na^+$ channels with a single-channel conductance of 18 pS (*12*) per cell. Comparison with the cell capacitance indicates a current density of 9.0 pA/pF and a density of $Na^+$ channels that are active during the peak current of 0.1 per square micrometer of cell surface area. In contrast, similar estimates of the density of active $Na^+$ channels at peak current indicate that mouse neuroblastoma cells have a $Na^+$ channel density of approximately 2 to 20 channels per square micrometer (*13, 14*), and the cell bodies of rat central neurons have a channel density of 3 to 10 channels per square micrometer (*15–17*). The expression of active $Na^+$ channels in these transfected cell lines is much lower than that in neuronal cells.

The voltage dependence of activation of the $Na^+$ currents is consistent with the properties of $Na^+$ channels encoded by the $R_{IIA}$ α subunit cDNA. In average current-voltage (*I-V*) relations for peak inward $Na^+$ current from PVA1 cells (Fig. 2A), inward $Na^+$ current is first evident near −20 mV, and peak inward current is achieved between +10 and +20 mV. Activation curves derived from peak currents (Fig. 2B) have half-activation voltages near 0 mV. The peak $Na^+$ current is activated at a voltage that is 10 to 20 mV more positive than peak $Na^+$ currents recorded under similar conditions in cultured embryonic rat brain neurons (*17*), in different recording solutions in

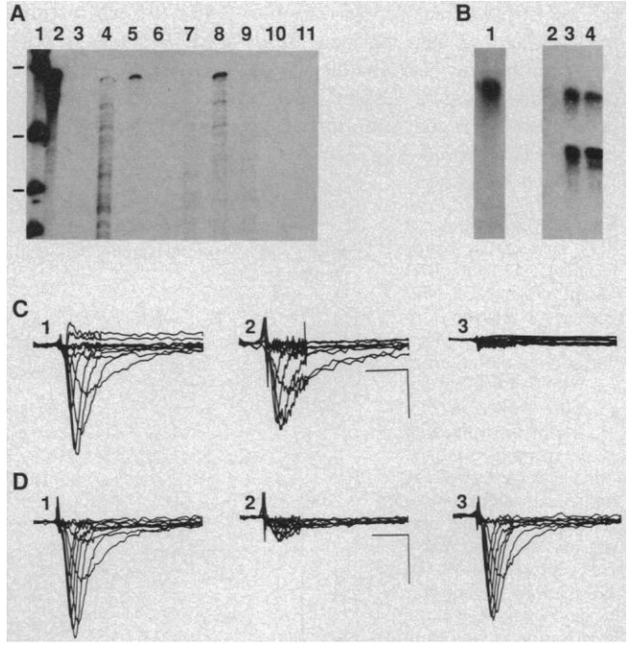


**Fig. 1.** Functional expression of rat brain $Na^+$ channels in transfected CHO cells. (**A**) RNase protection. Autoradiogram of $\alpha_{IIA}$ transcripts protected from RNase digestion in seven independent transfected CHO lines. Cytoplasmic RNA was isolated from detergent-solubilized CHO cells by NaOAc, *p*H 5, and precipitated by ethanol (*30*). CHO RNA (15 μg), 10 μg of tRNA, or 2 μg of brain poly(A)$^+$ RNA was hybridized to a 781-nt probe containing nucleotides 50 to 831 (7) of the $\alpha_{IIA}$ mRNA and treated with RNase A and RNase T1 as described (*31*). Denatured RNA duplexes were electrophoresed on a 5% polyacrylamide gel. Lane 1, size markers (tick marks indicate 1018, 516/506, and 394 nt); lane 2, probe; lane 3, tRNA; lane 4, brain poly(A)$^+$ RNA; lanes 5 to 11, transfected CHO lines PVA1 to PVA7, respectively. (**B**) Messenger RNA blot. CHO cells were transfected with pVA222 or the pECE vector, and stable cell lines were established as described (*9*). RNA was isolated from cells by homogenization in guanidine thiocyanate and centrifugation through CsCl (*32*). Total RNA (10 μg) was electrophoresed in agarose gels containing 2.2*M* formaldehyde, transferred to nitrocellulose, and hybridized to a cRNA probe containing an insert spanning nucleotides 3361 to 5868 of the $R_{IIA}$ α subunit (7). Hybridization was performed in a solution of 6× saline sodium citrate (SSC), 50% formamide, 50 m*M* tris-HCl, 10× Denhardt's solution, and 0.5% SDS at 68°C. After hybridization, the blot was washed at room temperature in 2× SSC, 0.5% SDS, and in 0.2× SSC, 0.5% SDS at 68°C. After washing, the nitrocellulose filters were exposed for autoradiography for 1 hour (lane 1) or 8 hours (lanes 2 to 4) at −80°C. Lane 1, total brain RNA; lane 2, CP1 RNA; lane 3, PVA4 RNA; and lane 4, PVA1 RNA. (**C**) Sodium currents in PVA1 (panel 1), PVA4 (panel 2), and CP1 (panel 3) cells. Inward $Na^+$ currents were recorded during step depolarizations to −38, −29, −19, −10, 0, 19, 38, 57, 77, and 86 mV for 16 ms from a holding potential of −67 mV. Pulses +77 and +86 mV are omitted for PVA4 cell. Each voltage step was preceded by a 200-ms long prepulse to −100 mV. Calibration: 2 ms; 100 pA. (**D**) Families of $Na^+$ currents in PVA1 cells evoked by voltage steps ranging from −40 to +50 mV (in 10-mV steps) before (panel 1), during (panel 2), and after (panel 3) exposure to 100 n*M* TTX. Calibration: 2 ms; 100 pA.

acutely isolated brain neurons (*15, 16*), or in oocytes injected with brain polyadenylated [poly(A)$^+$] mRNA (*7*), $R_{II}$ mRNA (*4*), or $R_{III}$ mRNA (*5*). A similar voltage dependence was observed in every PVA1 and PVA4 cell that was studied. As in CHO cells, injection of $R_{IIA}$ α subunit mRNA into *Xenopus* oocytes yields $Na^+$ channels with peak currents at +10 to +20 mV (*7*). The relatively positive voltage dependence of activation of $R_{IIA}$ $Na^+$ channels expressed in either oocytes or CHO cells results from a single conservative amino acid change from leucine to phenylalanine at position **860** in putative transmembrane segment IIS4 (*17a*).

The decay of $Na^+$ currents during a sustained depolarization was rapid in PVA1 cells with a $\tau_{1/2}$ of 0.7 ms at +10 mV (Fig. 2C). Inactivation time constants in PVA1 cells were similarly rapid at all potentials tested (Fig. 2D). Steady-state inactivation of the $Na^+$ current had an unusually steep voltage dependence in PVA1 cells (Fig. 2B and Table 1). There was virtually no resting inactivation at our normal holding potential of −67 mV, whereas depolarization to −50 mV resulted in half-maximal steady-state inactivation. The $Na^+$ channels were completely inactivated by −30 mV, and little or no overlap of the activation and inactivation curves was observed (Fig. 2B). Steady-state $Na^+$ current resulting from such overlap may contribute to the generation of bursts of action potentials (*18*). $R_{IIA}$ $Na^+$ channels are unlikely to contribute significantly to this aspect of neuronal excitability.

The time course of inactivation of $Na^+$ currents resulting from expression of $R_{IIA}$ $Na^+$ channels in CHO cells is comparable to that of $Na^+$ currents in rat embryonic brain neurons in cell culture (*17*) or acutely dissociated adult rat central neurons (*15, 16*). In contrast, $Na^+$ currents resulting from expression of $R_{IIA}$ in oocytes inactivate much more slowly (*7*). Sodium currents during a depolarization to +10 mV were compared for $Na^+$ channels expressed in PVA1 cells (solid trace) or in oocytes (dotted trace) (Fig. 2C) (*7*). In CHO cells, currents inactivated within 1 to 2 ms, whereas in oocytes, inactivation was incomplete by the end of a 16-ms pulse. Recovery from inactivation in CHO cells was also rapid because no decrease in peak currents was seen during trains of pulses applied at 5 Hz. Sodium currents in oocytes injected with only the $R_{IIA}$ α subunit mRNA diminish when stimulated with a similar protocol (*19*). A protein of low molecular weight can act to make the oocyte environment equivalent to that of the CHO cell (*7*). Candidates for this low molecular weight protein include $\beta_1$ or $\beta_2$ subunits, whose function remains unknown, and modulatory proteins such as protein kinases or enzymes involved in other post-translational modifications. Our results show that this low molecular weight protein that is necessary for rapid inactivation kinetics of $R_{IIA}$ $Na^+$ channels in oocytes (*7*) must either be endogenous or unnecessary in the environment of the CHO cell.

Sodium currents mediated by native $Na^+$ channels are blocked by TTX and saxitoxin acting at neurotoxin receptor site 1, are persistently activated by veratridine, batrachotoxin, and other lipid-soluble toxins acting at neurotoxin receptor site 2, and are markedly potentiated and prolonged by polypeptide α-scorpion toxins and sea anemone toxins acting at neurotoxin receptor site 3 (*1*). To test whether functional receptor sites for these three classes of toxins are present on $R_{IIA}$ α subunits, we examined the effect of representative toxins on $Na^+$ currents in transfected CHO cells. Tetrodotoxin inhibits $Na^+$ currents in PVA1 (Fig. 1D) and PVA4 cells. The **80%** inhibition observed at 100 n*M* is consistent with a dissociation constant of 25 n*M*, in close agreement with biochemical studies of brain $Na^+$ channels (*20*).

Veratridine and related lipid-soluble neurotoxins that act at neurotoxin receptor site 2 preferentially bind to activated $Na^+$ channels and cause persistent activation (*21–25*). Their action is enhanced by repetitive activation of $Na^+$ channels. We examined the effect of veratridine on $Na^+$ currents recorded in PVA1 cells (Fig. 3). The protocol was designed to give a progressive increase in the number of veratridine-modified channels. Veratridine caused a sustained component of inward $Na^+$ current that was not inactivated during the 16-ms test pulses. In addition, there was a pulse-by-pulse increase in the sustained inward current recorded on return to the holding potential after each pulse (Fig. 3A, arrow). This current represents inward $Na^+$ movement through persistently activated $Na^+$ channels, which is increased at the negative holding potential (−100 mV) in comparison to the test potential because of the greater electrical driving force for $Na^+$ influx.

Veratridine acts on native $Na^+$ channels by preventing inactivation and by shifting activation to more negative potentials (*21–25*). The combination of these effects prevents channel closing on repolarization and causes the sustained inward $Na^+$ current. We also found that the voltage dependence of activation for veratridine-modified $Na^+$ channels expressed from $R_{IIA}$ cDNA was shifted to more negative membrane potentials. A population of veratridine-modified channels was generated by ten successive

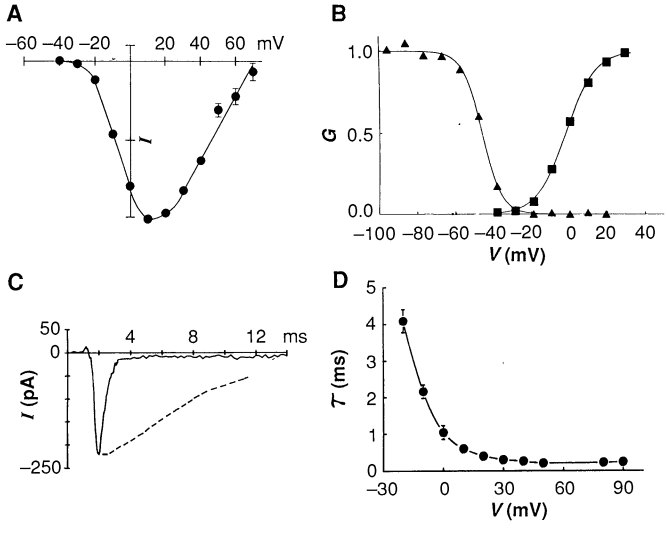


**Fig. 2.** Properties of $Na^+$ currents in transfected CHO cells. (**A**) Mean, normalized $Na^+$ current *I-V* relation from PVA1 cells. Peak $Na^+$ currents measured from current families similar to those shown in Fig. 1C were normalized to peak current, averaged on a voltage-by-voltage basis, and plotted as a function of voltage during the test pulse. Error bars represent SEM. (**B**) Normalized conductance-voltage (*G-V*) and inactivation curves from a PVA1 cell. *G-V* curves were obtained from $Na^+$ current families recorded as in Fig. 1C. Conductances, *G* (squares), were obtained from normalized peak current values, *I*, the test pulse voltage *V*, and the measured *I-V* curve reversal potential $V_{rev}$, according to the equation: $G(V) = I/(V - V_{rev})$. Inactivation curve was determined by using 200-ms long prepulses to the indicated membrane potentials followed by a test pulse to +10 mV. Normalized peak currents are plotted as a function of prepulse potential (triangles). Curves through the points are least-squares fits normalized to $1/\{1 + \exp[(V - V_{0.5})/k]\}$, where $V_{0.5}$ is the voltage of half-activation and *k* gives the steepness of voltage dependence. Best fit values were as follows: Activation, $V_{0.5}$ = +2.0 mV, $k$ = −7.55 mV; inactivation, $V_{0.5}$ = −45.96, $k$ = 5.06. (**C**) Comparison of the time courses of $Na^+$ currents mediated by $R_{IIA}$ α subunits expressed in PVA1 cells and in *Xenopus* oocytes. Solid trace, inward current evoked by a voltage pulse to +10 mV in a PVA1 cell. Broken trace, approximate time course of $I_{Na}$ in a *Xenopus* oocyte at the same test potential, as reported (*7*). (**D**) Time constants of macroscopic inactivation of $I_{Na}$. Points were obtained by least-squares fits of single exponentials to the decline of $I_{Na}$ during depolarizations. Points represent the means of six to nine determinations except at +80 and +90 mV where $n$ = 2. Error bars (±SEM) in (A) and (D) are not shown when smaller than the symbol size.

depolarizations as in Fig. 3A. After each pulse train, a test pulse was applied to a variable test potential. The voltage dependence of veratridine-modified $Na^+$ channels obtained in this way was strongly displaced in the negative direction in comparison to control (Fig. 3B), as has been reported for veratridine acting on native $Na^+$ channels (*22, 25*).

Polypeptide toxins from Old World scorpions, called α-scorpion toxins, remove or greatly slow $Na^+$ channel inactivation (*1, 14, 26–28*). Purified α-toxin from the scorpion *Leirus quinquestriatus* slowed inactivation of $R_{IIA}$ $Na^+$ channels expressed in CHO cells (Fig. 3C). The rapid inactivation of $Na^+$ currents at positive test potentials is most strikingly affected. The slowing of inactivation allowed greater peak $Na^+$ currents to be attained at each test potential (Fig. 3C) and caused a shift of the voltage dependence of $Na^+$ channel activation to more negative membrane potentials (Fig. 3D). These effects are consistent with the actions of α-scorpion toxin on other mammalian nerve cells (*14, 28*).

Our results show that only the α subunit of the $Na^+$ channel is necessary for expression of functional $Na^+$ channels in CHO cells. Sodium channels composed of this single subunit are inhibited by TTX acting at neurotoxin receptor site 1 and persistently activated by veratridine acting at neurotoxin receptor site 2. Their inactivation is slowed by *Leiurus* α-scorpion toxin acting at neurotoxin receptor site 3. These results show that the $R_{IIA}$ α subunit cDNA is sufficient to encode neurotoxin receptor sites 1 through 3 in functional form.

*Leiurus* toxin binds to a site near the contact regions of the α and $\beta_1$ subunits and photoreactive derivatives covalently label both of these subunits while specifically bound (*1*). The site of covalent attachment of *Leiurus* toxin to the α subunit has been localized to the major extracellular loop in homologous domain I of the α subunit (*29*). Our data provide evidence that the functional receptor site for α-scorpion toxins is located on the α-subunit and confirm that the primary binding site for that toxin is on, not just near, the α subunit.

The stable transfection of ion channel genes into mammalian cell lines offers important experimental advantages. It will allow the study of a single ion channel subtype in cells of simple morphology and constant genetic background. In addition, individual ion channel subtypes can be expressed in diverse biological environments that may alter their functional properties. Expression of individual ion channel subtypes in somatic cell lines with different receptor and second messenger pathways may provide a novel approach to analysis of the regulatory mechanisms controlling channel activity.

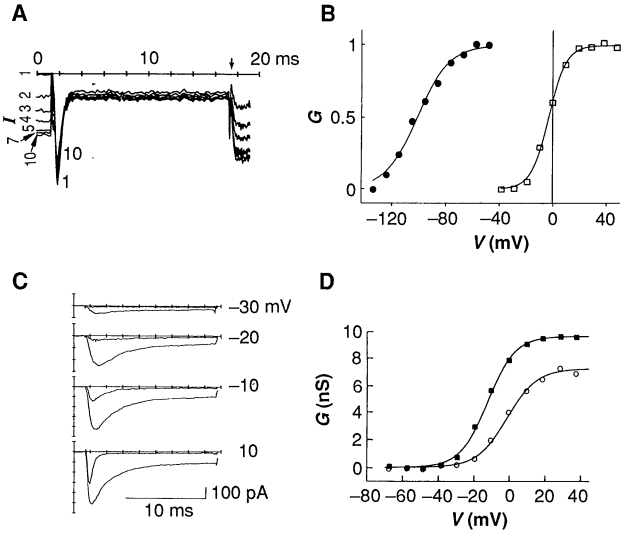


**Fig. 3.** Toxin effects on $Na^+$ channels expressed in CHO cells. (**A**) Currents recorded during ten successive depolarizations from a holding potential of −100 to +20 mV applied at 5 Hz in the presence of 100 μ*M* veratridine. Current traces shown were recorded during pulses 1 to 5, 7, and 10 as indicated next to each trace. Each trace represents the pulse-wise average of five successive pulse trains separated by 30-s to 1-min quiescent intervals. Similar trains of control pulses caused no pulse-wise changes in peak or holding current. (**B**) Voltage dependence of veratridine-modified $Na^+$ channels. Control *G-V* curve (open squares) was obtained as described in Fig. 2B. During exposure to 100 μ*M* veratridine, approximate mean conductances (filled circles) were obtained by developing a population of veratridine-modified channels by using a train of ten successive, 2-ms-long pulses as in (A). Membrane potential was then stepped to −160 mV for 17 ms followed by pulses to the test potentials shown. Veratridine-modified channels close slowly in comparison to the 17 ms spent at −160 mV and therefore remain open during the subsequent test pulses. Peak current values were measured and transformed into normalized conductances as in Fig. 2B. (**C**) Effect of the α-scorpion toxin from *L. quinquestriatus* on $Na^+$ currents. The time course of inward $Na^+$ current was measured at the indicated test potentials (at right) before and during exposure to purified *L. quinquestriatus* toxin (*33*). At each membrane potential, the larger $Na^+$ current was recorded in the presence of *L. quinquestriatus* toxin. After control recordings, 2 μl of 70 μ*M* toxin was added near the cell. Toxin concentration for uniform distribution in the bath volume was 140 n*M*. (**D**) *G-V* relations before and during exposure to *L. quinquestriatus* toxin. Same experiment as in (C). Conductance values (unnormalized) and fit curves were obtained as in Fig. 2B. Best fit values were as follows: control (open circles), $V_{0.5}$ = −0.45 mV, $k$ = −8.9 mV; *L. quinquestriatus* toxin (closed squares), $V_{0.5}$ = −9.9 mV, $k$ = −7.7 mV.


REFERENCES AND NOTES

1. W. A. Catterall, *Annu. Rev. Biochem.* **55**, 953 (1986); *Science* **242**, 50 (1988); *ISI Atlas Sci. Pharmacol.* **2**, 190 (1988).
2. M. Noda *et al.*, *Nature* **320**, 188 (1986).
3. T. Kayano *et al.*, *FEBS Lett.* **228**, 187 (1988).
4. M. Noda *et al.*, *Nature* **322**, 826 (1986).
5. H. Suzuki *et al.*, *FEBS Lett.* **228**, 195 (1988).
6. A. L. Goldin *et al.*, *Proc. Natl. Acad. Sci. U.S.A.* **83**, 7503 (1986).
7. V. J. Auld *et al.*, *Neuron* **1**, 449 (1988).
8. The full-length rat IIA cDNA (*7*) was inserted into the Bgl II site of the mammalian expression vector pECE (*9*) to generate pVA222. In this construct transcripts encoding the rat IIA cDNA originate from the simian virus 40 early promoter. The pECE (10 μg) and pSV2neo (2 μg) vectors were cotransfected into CHO cells as a calcium phosphate precipitate [P. J. Southern and P. Berg, *J. Mol. Appl. Genet.* **1**, 37 (1982)]. The transfected cells were treated with G418 (400 μg/ml) to select stable cell lines essentially as described by Ellis *et al.* (*9*). Seven stable cell lines were obtained (PVA1 through PVA7).
9. L. Ellis *et al.*, *Cell* **45**, 721 (1986).
10. O. P. Hamill *et al.*, *Pfluegers Arch.* **391**, 85 (1981).
11. Transfected CHO cells were maintained in RPMI medium supplemented with 10% fetal calf serum and selected continuously in the presence of G418 (400 μg/ml). Cells were studied with the whole cell variant of the patch clamp technique. Electrodes were formed from hematocrit tubing (VWR Scientific, Philadelphia, PA) and had resistances of 1 to 1.5 megohms when filled with standard intracellular solutions. Currents were recorded with a standard patch clamp amplifier (List EPC7). Linear leak and capacitance were cancelled internally. Approximately 70% of series resistance was compensated. Remaining linear capacitance and leak were cancelled by subtracting scaled pulses obtained in a voltage range where no inward currents are activated. For some pulses, capacity transients still saturated at the pulse transitions and resulted in incomplete transient cancellation. *I-V* curves in the absence of $I_{NA}$ were linear. In most cases 4 to 16 individual current records were averaged to produce the traces shown. Currents were filtered at 7 to 10 kHz, digitized at 20 μs per point, and stored for later analysis (Basic-Fastlab, Indec Systems, Sunnyvale, CA). Extracellular solution contained 150 m*M* NaCl, 5 m*M* KCl, 1.5 m*M* $CaCl_2$, 1 m*M* $MgCl_2$, 10 m*M* Na Hepes, and 5 m*M* glucose, *p*H 7.4. Intrapipette solution for transfected CHO cells was 90 m*M* cesium aspartate, 60 m*M* CsCl, 5 m*M* NaCl, 5 m*M* Na EGTA, and 2 m*M* Mg ATP (adenosine triphosphate), *p*H 7.4. TTX (Sigma) and veratridine (Aldrich) were maintained in aqueous stock solutions.
12. W. Stuhmer *et al.*, *Eur. Biophys. J.* **14**, 131 (1987).
13. W. H. Moolenaar and I. Spector, *J. Physiol. (London)* **278**, 265 (1978).
14. T. Gonoi, B. Hille, W. A. Catterall, *J. Neurosci.* **4**, 2836 (1984).
15. P. Sah *et al.*, *J. Gen. Physiol.* **91**, 373 (1988).
16. J. Huguenard, O. P. Hamill, D. A. Prince, *J. Neurophysiol.* **59**, 778 (1988).
17. J. Coombs *et al.*, *Biophys. J.* **53**, 542a (1988).
17a. V. J. Auld *et al.*, *Proc. Natl. Acad. Sci. U.S.A.* **87**, 323 (1990).
18. C. E. Stafstrom *et al.*, *J. Neurophysiol.* **53**, 153 (1985).
19. A. L. Goldin *et al.*, *Soc. Neurosci. Abstr.* **14**, 598 (1988).
20. W. A. Catterall, C. S. Morrow, R. P. Hartshorne, *J. Biol. Chem.* **254**, 11379 (1979).
21. W. Ulbricht, *Ergeb. Physiol. Biol. Chem. Exp. Pharmakol.* **61**, 18 (1969).
22. M. D. Leibowitz, J. B. Sutro, B. Hille, *J. Gen. Physiol.* **87**, 25 (1986).
23. J. B. Sutro, *ibid.*, p. 1.
24. T. A. Rando, G. K. Wang, G. R. Strichartz, *J. Pharmacol. Exp. Ther.* **29**, 467 (1986).

25. ———, *J. Gen. Physiol.* **93**, 43 (1989).
26. E. Kopenhofer and H. Schmidt, *Pfluegers Arch.* **303**, 133 (1968).
27. G. K. Wang and G. Strichartz, *J. Gen. Physiol.* **86**, 739 (1985).
28. G. E. Kirsch, A. Skattebøl, L. Possani, A. M. Brown, *ibid.* **93**, 67 (1989).
29. F. J. Tejedor and W. A. Catterall, *Proc. Natl. Acad. Sci. U.S.A.* **85**, 8742 (1988).
30. C. D. Rasmussen, R. C. M. Simmen, E. A. MacDougall, A. R. Means, *Meth. Enzymol.* **139**, 642 (1987).
31. D. A. Melton, P. A. Kreig, M. R. Rebaliati, T. Maniatis, *Nucleic Acids Res.* **12**, 7035 (1984).
32. V. Glisin, R. Crkvenjakov, C. Byus, *Biochemistry* **13**, 2633 (1973).
33. W. A. Catterall, *J. Biol. Chem.* **251**, 5528 (1976).
34. We thank W. Newerly-Abranow for guidance and J. C. Roder for use of tissue-culture facilities and reagents. Supported by grants from the Medical Research Council of Canada and the Multiple Sclerosis Society of Canada to R.J.D., NIH research grants NS 15751 and NS 25704 to W.A.C., and a postdoctoral fellowship from the Multiple Sclerosis Society to J.O.

24 August 1989; accepted 20 November 1989

# Subcellular Calcium Transients Visualized by Confocal Microscopy in a Voltage-Clamped Vertebrate Neuron

ARTURO HERNÁNDEZ-CRUZ,* FRANCISCO SALA,† PAUL R. ADAMS

**Confocal laser-scanned microscopy and long-wavelength calcium ($Ca^{2+}$) indicators were combined to monitor both sustained and rapidly dissipating $Ca^{2+}$ gradients in voltage-clamped sympathetic neurons isolated from the bullfrog. After a brief activation of voltage-dependent $Ca^{2+}$ channels, $Ca^{2+}$ spreads inwardly, and reaches the center of these spherical cells in about 300 milliseconds. Although the $Ca^{2+}$ redistribution in the bulk of the cytosol could be accounted for with a radial diffusion model, local nonlinearities, suggesting either nonuniform $Ca^{2+}$ entry or spatial buffering, could be seen. After electrical stimulation, $Ca^{2+}$ signals in the nucleus were consistently larger and decayed more slowly than those in the cytosol. A similar behavior was observed when release of intracellular $Ca^{2+}$ was induced by caffeine, suggesting that in both cases large responses originate from $Ca^{2+}$ release sites near or within the nucleus. These results are consistent with an amplification mechanism involving $Ca^{2+}$-induced $Ca^{2+}$ release, which could be relevant to activity-dependent, $Ca^{2+}$-regulated nuclear events.**

THE SPATIAL DISTRIBUTION OF INTRACELLULAR $Ca^{2+}$ after excitation in nerve cells depends on the location and density of $Ca^{2+}$ channels, as well as buffering, sequestration, and release of $Ca^{2+}$ within the cytoplasm. The dynamics of intracellular $Ca^{2+}$ are relevant to the kinetics of $Ca^{2+}$-activated membrane conductances and other $Ca^{2+}$-regulated processes, such as transmitter release, release of intracellular $Ca^{2+}$, and activation of enzymes and genes (*1*). Time resolution in the order of milliseconds and spatial resolution in the micron range are required to monitor rapid local changes in the $Ca^{2+}$ concentration ($[Ca^{2+}]$) associated with nerve excitation and to thus overcome the blurring effects of diffusion. We have used confocal microscopy to monitor the redistribution of the intracellular $[Ca^{2+}]$ ($[Ca^{2+}]_i$) after the entry of $Ca^{2+}$ through voltage-gated $Ca^{2+}$ channels and its release from caffeine-sensitive intracellular stores (*2*).

Confocal fluorescence microscopy has several advantages over conventional microscopy for $Ca^{2+}$ imaging (*3*). (i) The narrower depth of field allows better visualization of intracellular details by eliminating out-of-focus signals. (ii) A substantially improved lateral spatial resolution is expected. (iii) Measurement errors due to path-length variations are minimized because a small and relatively constant volume of the cell is sampled throughout the focal plane. This last feature is particularly relevant, because currently available long-wavelength $Ca^{2+}$ indicators are not suitable for the determination of absolute $Ca^{2+}$ concentrations by ratio imaging (*4, 5*).

We measured the $[Ca^{2+}]_i$ of dissociated bullfrog sympathetic neurons under voltage-clamp conditions so as to allow precise control of transmembrane $Ca^{2+}$ influx. The $Ca^{2+}$ indicator fluo-3 (*4*) was used to monitor changes in $[Ca^{2+}]_i$. We rountinely used two image acquisition modes. In the frame-scanning mode (FSM), an image frame can be collected in 1 s. Steady or slowly changing gradients throughout the cell were monitored with this method. In the line-scanning mode (LSM), the monitored region of the cell was reduced to a narrow "slot" by scanning the beam in only one spatial dimension. Because of the small number of pixels acquired per cycle (384 in most cases), a temporal resolution of 5 ms or less was achieved, without the loss of spatial resolution. LSM images contain detailed spatiotemporal information of the changes in $[Ca^{2+}]_i$ that occur during the formation of the image. Thus, the changes in $[Ca^{2+}]$ across the cell (horizontal axis) can be followed as a function of time (vertical axis).

In the example shown in Fig. 1, a brief $Ca^{2+}$ current produced an inward "wave" of increased $[Ca^{2+}]$ that reached the center of the cell in ~300 ms. Subsequently, $[Ca^{2+}]$ equilibrated across the cell, returning to resting values within 6 to 8 s. Although the $[Ca^{2+}]$ transients in the periphery were faster and larger than those at the center of the cell (Fig. 1, G and H), those near the cell membrane, although rapid, were attenuated because of cell curvature. Both $Ca^{2+}$ transients and $Ca^{2+}$ currents were absent in $Ca^{2+}$-free external solution or after superfusion with 100 $\mu M$ $Cd^{2+}$. These observations represent, to our knowledge, the first experimental confirmation of the stimulus-induced, rapidly dissipating spatial $Ca^{2+}$ gradients in the cytoplasm that had been previously modeled theoretically (*6*).

The basic features of $Ca^{2+}$ dynamics after a brief period of $Ca^{2+}$ entry could be mimicked with a diffusion model (*7*). Our formulation differs from previous radial diffusion models (*6*) in that it includes both mobile and stationary $Ca^{2+}$ buffers (one of the mobile buffers being the dye itself), as well as a $Ca^{2+}$ extrusion mechanism (*8*). Peripheral $Ca^{2+}$ transients decay in two phases: an early phase, lasting about 300 ms and due mainly to diffusional redistribution across the cell, and a late phase, lasting for seconds and reflecting slow buffering and membrane extrusion. Spatial gradients across the cell are absent during the late phase. Under our experimental conditions and on the time scale of interest, fluo-3 seems to be the dominant fast $Ca^{2+}$ buffer. The model predicts that the early phase would be slower and the late phase would be more rapid in the absence of dye; this follows from the $Ca^{2+}$-transporting properties of the diffusible exogenous buffer. Also, $Ca^{2+}$ transients should be considerably larger throughout the cell in the absence of dye. A complex interplay between mobility, capacity, and affinity of intracellular buffers determines the time course, magnitude, and spreading of $Ca^{2+}$ signals in the cytoplasm (*7*).

Howard Hughes Medical Institute, Department of Neurobiology and Behavior, State University of New York at Stony Brook, Stony Brook, NY 11794.

*To whom correspondence should be addressed at Department of Neurosciences, Roche Institute of Molecular Biology, Nutley, NJ 07110.
†Present address: Departamento de Neuroquímica, Universidad de Alicante, Alicante, Spain.